AGU PUBLICATIONS

Geophysical Research Letters

RESEARCH LETTER
10.1002/2014GL060607

Key Points:
- Deformation mechanism map for orthopyroxene is constructed
- Diffusion creep of orthopyroxene is important over a wide range of conditions

Correspondence to:
R. H. C. Bruijn,
bruijn@levee.wustl.edu

Citation:
Bruijn, R. H. C., and P. Skemer (2014), Grain-size sensitive rheology of orthopyroxene, *Geophys. Res. Lett.*, *41*, doi:10.1002/2014GL060607.

Received 20 MAY 2014
Accepted 3 JUL 2014
Accepted article online 4 JUL 2014

Grain-size sensitive rheology of orthopyroxene

Rolf H.C. Bruijn[1] and Philip Skemer[1]

[1]Department of Earth and Planetary Sciences, Washington University in St. Louis, Saint Louis, Missouri, USA

Abstract The grain-size sensitive rheology of orthopyroxene is investigated using data from rheological and microstructural studies. A deformation mechanism map is constructed assuming that orthopyroxene deforms by two independent mechanisms: dislocation creep and diffusion creep. The field boundary between these mechanisms is defined using two approaches. First, experimental data from Lawlis (1998), which show a deviation from non-linear power law behavior at low stresses, are used to prescribe the location of the field boundary. Second, a new orthopyroxene grain-size piezometer is used as a microstructural constraint to the field boundary. At constant temperature, both approaches yield sub-parallel field boundaries, separated in grain size by a factor of only 2–5. Extrapolating to lithospheric conditions, the deformation mechanism transition occurs at a grain size of ~150–500 μm, consistent with observations from nature. As the transition from dislocation to diffusion creep may promote shear localization, grain-size reduction of orthopyroxene may play a prominent role in plate-boundary deformation.

1. Introduction

Orthopyroxene ($(Mg,Fe)_2Si_2O_6$) is the second most abundant mineral in Earth's upper mantle after olivine [*Ringwood*, 1975] and is likely to be an important constituent of other planetary lithospheres [*Sanloup et al.*, 1999; *Mocquet et al.*, 2011]. Yet in comparison to olivine relatively little is known about its rheological behavior. Due to the complex phase stability of $(Mg,Fe)_2Si_2O_6$ at low pressure [*Presnall*, 1995], there are few experimental deformation studies on orthoenstatite, the stable polymorph in the upper mantle. Furthermore, these experiments are largely limited to the conditions where grain-size insensitive dislocation creep is the dominant deformation mechanism [*Raleigh et al.*, 1971; *Carter et al.*, 1972; *Ross and Nielsen*, 1978; *Hitchings et al.*, 1989; *Lawlis*, 1998; *Ohuchi et al.*, 2011]. Sheared orthopyroxene porphyroclasts in lower crustal and upper mantle tectonites have been frequently observed to deform by dislocation creep [e.g., *Nicolas et al.*, 1971; *Kohlstedt and Vander Sande*, 1973; *Etheridge*, 1975; *Boudier*, 1978; *Christensen and Lundquist*, 1982; *Skemer et al.*, 2006; *Soustelle et al.*, 2009; *Tikoff et al.*, 2010]. However, there is also abundant microstructural evidence that a grain-size sensitive (GSS) deformation mechanism, for example diffusion creep, may play an important role in the deformation of the lower crust [*Kanagawa et al.*, 2008; *Raimbourg et al.*, 2008] and upper mantle (Figure 1) [*Boullier and Gueguen*, 1975; *Dijkstra et al.*, 2002; *Skemer and Karato*, 2008; *Skemer et al.*, 2010; *Toy et al.*, 2010; *Linckens et al.*, 2011a; *Hidas et al.*, 2013].

In this study we apply two independent approaches to constrain the deformation conditions where GSS deformation of orthopyroxene may be important. The first approach employs existing rheological data. We revisit some of the previous experimental work on orthoenstatite by *Lawlis* [1998] to determine the conditions at which a deviation from power law creep is observed. These data are used to define the onset of GSS deformation at low stresses. The second approach uses microstructural constraints. We apply the field boundary hypothesis *De Bresser et al.*, 1998, 2001] and the recently determined grain-size piezometer for orthopyroxene [*Linckens et al.*, 2014] to determine the deformation conditions at which dislocation creep and GSS creep contribute equally to the total rate of deformation. Both sets of data are used to construct a deformation mechanism map [cf. *Frost and Ashby*, 1982] and constrain underlying flow laws for orthopyroxene at temperatures of 1200°C –1250°C. We demonstrate that the two independent approaches provide nearly identical constraints on the range of conditions where grain-size sensitive deformation is predicted to be the dominant mode of deformation in orthopyroxene.

2. Methods

2.1. Deformation Mechanism Maps

Rocks at high temperature and pressure may deform by several different ductile deformation mechanisms. Deformation mechanism maps show the range of conditions where each mechanism exerts primary control

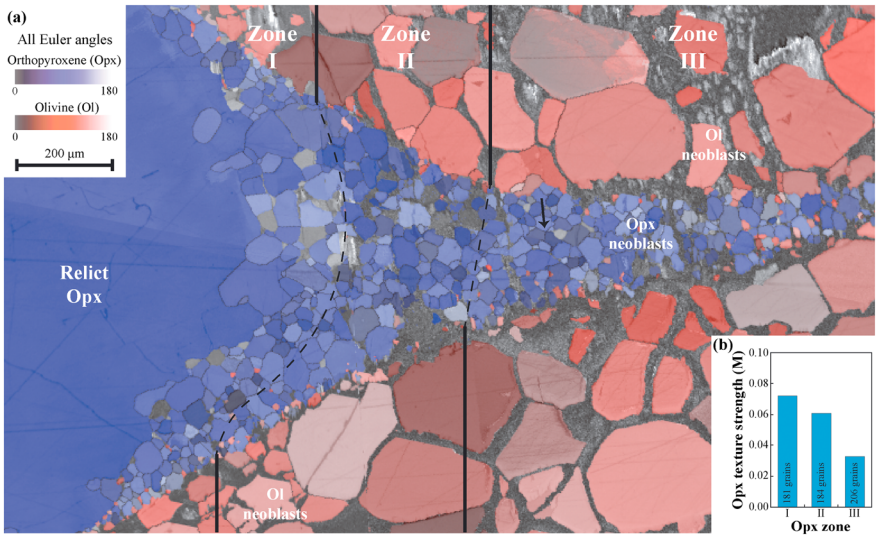

Figure 1. (a) Electron backscatter diffraction (EBSD) map of a nominally dry partially recrystallized orthopyroxene clast surrounded by recrystallized olivine grains in a highly sheared mantle xenolith from *Skemer and Karato* [2008]. Orthopyroxene neoblasts exhibit straight grain boundaries and no evidence for internal deformation, indicating that the motion of dislocations played a minor role during the deformation of the neoblasts. As the orthopyroxene neoblasts occasionally give rise to four-grain junctions (black arrow), grain-size sensitive creep is inferred as the most important deformation mechanism within the neoblasts. (b) Bar graph for the texture strength, expressed using the M-index [*Skemer et al*., 2005], of the orthopyroxene neoblasts in zones I to III. The neoblasts in the recrystallized tail show a progressive weakening of the crystallographic preferred orientation (CPO) as the distance from the relict orthopyroxene clast increases, which is also inferred to be a consequence of grain-size sensitive deformation. The curved shape of the boundaries between zone I and II was specifically chosen to reflect the curvature of the relict clast.

on the total rate of deformation [*Frost and Ashby*, 1982]. Deformation mechanism maps are typically constructed using empirical flow laws for a particular mineral. A generic flow law for describing high-temperature rheology is:

$$\dot{\varepsilon} = A\sigma^n d^{-p} \exp\left(-\frac{H}{RT}\right) \tag{1}$$

where $\dot{\varepsilon}$, σ, d, R, and T are the strain rate, stress, grain size, gas constant, and temperature of deformation, respectively. A, a pre-exponential factor, constants n and p, and the pressure-dependent activation enthalpy H depend on the mineral phase and mechanism of deformation. The field boundary between two deformation mechanisms is defined as the locus of points where the strain rates of the two independent mechanisms are equal. For a material that deforms by dislocation creep and diffusion creep, the field boundary is defined as:

$$\dot{\varepsilon}_{dis} = \dot{\varepsilon}_{dif} \tag{2}$$

where subscripts "*dis*" and "*dif*" refer to dislocation creep and diffusion creep mechanisms, respectively. At constant temperature, pressure, and composition, the boundary between the two mechanisms depends only on stress and grain size.

2.2. Rheological Approach

While there are relatively few experimental data on the rheology of orthopyroxene in the orthoenstatite stability field, a pioneering study by *Lawlis* [1998] provides some valuable data over a wide range of pressure, temperature, and stress conditions. Most of Lawlis' experiments were conducted at conditions where deformation is dominated by dislocation creep. A best fit to these data gives a flow law for orthoenstatite of the form given in equation (1):

$$\dot{\varepsilon}_{dis} = A_{dis}\sigma^{n_{dis}} \exp\left(-\frac{H_{dis}}{RT}\right) \tag{3}$$

Parameters reported by *Lawlis* [1998] are provided in Table 1.

Table 1. Flow Law and Microstructural Parameters for Orthoenstatite Used to Construct Deformation Mechanism Maps

Parameter[a]	Value[b]	Source
A_{dis} (s^{-1} $MPa^{-2.9}$)	6.92×10^{8}	*Lawlis* [1998]
n_{dis}	2.9	*Lawlis* [1998]
H_{dis} (kJ mol^{-1})	600	*Lawlis* [1998]
α (MPa $\mu m^{-1.308}$)	$2939^{+1673/-1066}$	*Linckens et al.* [2014]
β	$1.308^{\pm 0.01}$	*Linckens et al.* [2014]
P	$2.49^{\pm 0.01}$	Microstructural approach
n_{gss}	1	*Coble* [1963]
d (μm)	8 ± 2	*Lawlis* [1998]
C_r *(1200°C)* (s^{-1} MPa^{-1} μm^3)	$1.9^{\pm 0.3} \times 10^{-6}$	Rheological approach
C_r *(1250°C)* (s^{-1} MPa^{-1} μm^3)	$7.0^{\pm 4.7} \times 10^{-6}$	Rheological approach
C_m *(1200°C)* (s^{-1} MPa^{-1} μm^3)	$1.42^{+1.93/-0.81} \times 10^{-6}$	Microstructural approach
C_m *(1250°C)* (s^{-1} MPa^{-1} μm^3)	$7.11^{+9.59/-4.09} \times 10^{-6}$	Microstructural approach

[a]Subscripts "*dis*" and "*gss*" denote values for dislocation creep and GSS creep, respectively. Grain sizes, stresses, and associated pre-exponentials have dimensions of μm and MPa.
[b]Superscript values in italic represent upper (+) and lower (−) or both (±) bounds, which originate from uncertainties in the orthopyroxene grain-size piezometer (microstructural approach) or represent the one-sigma standard deviation (rheological approach).

In two sets of creep tests on polycrystalline orthoenstatite ($En_{91;}$ experiments PI-512 and PI-539), *Lawlis* [1998] observed a deviation from non-linear power law behavior at low stresses (Figure 2). This observation suggests that there was a significant contribution from another deformation mechanism at these conditions, such as diffusion creep or dislocation accommodated grain-boundary sliding. This small number of low stress creep tests, while not included in the analysis leading to the dislocation creep flow law (equation (3)), nonetheless contain a valuable insight into the onset of a grain-size sensitive deformation mechanism. In our analysis of these data we assume that the total strain rate ($\dot{\varepsilon}_{tot}$) is the sum of two independent deformation mechanisms:

$$\dot{\varepsilon}_{tot} = \dot{\varepsilon}_{dis} + \dot{\varepsilon}_{gss} \tag{4}$$

Subtracting the contribution of dislocation creep ($\dot{\varepsilon}_{dis}$) from the total strain rate ($\dot{\varepsilon}_{tot}$) gives an excess strain rate that we attribute to some form of GSS deformation ($\dot{\varepsilon}_{gss}$). Because there are few data at these conditions it is not possible to distinguish between different GSS deformation mechanisms. Therefore, we make the simplifying assumption that the GSS rheology inferred at these conditions is a form of diffusion creep, in which strain rate is proportional to stress and inversely proportional to grain size to the power of three [*Coble*, 1963]. Hence, the grain-size sensitive rheology can be described by a reduced version of equation (1):

$$\dot{\varepsilon}_{gss} = C_r(T)\sigma d^{-3} \tag{5}$$

The pre-exponential term A_{gss} and the temperature-dependent Arrhenius term (exp $(-H/RT)$), are combined into a single temperature-dependent constant $C_r(T)$, where the subscript "*r*" refers to the rheological approach. Grain size is not well constrained by *Lawlis* [1998] but is estimated from backscatter electron images using the mean-intercept method to be approximately 8 ± 2 μm. As the total strain in these experiments is small, grain size is assumed to be constant. Using this grain size and the reported steady state stresses, $C_r(T)$ is calculated for each creep test (Figure 2). For inclusion in the calculation, $\dot{\varepsilon}_{gss}$ is required to be at least 18% of the total strain rate. This threshold was chosen to maximize the number of reliable data in our calculation. Experiments PI-512 and PI-539 included creep tests at temperatures of 1200°C and 1250°C. An average value for $C_r(T)$ is determined at each temperature (Table 1). Using the flow law for dislocation creep (equation (3)) and diffusion creep (equation (5)), we construct deformation mechanism maps at temperatures of 1200°C and 1250°C following the method of *Frost and Ashby* [1982] (Figure 3).

2.3. Microstructural Approach

The steady-state grain size of a material that is dynamically recrystallized has been shown to depend primarily on the magnitude of the flow stress [*Twiss*, 1977; *Derby and Ashby*, 1987; *Shimizu*, 1998] or a non-zero fraction of the total deformation work [*Bercovici and Ricard*, 2005; *Austin and Evans*, 2007; *Rozel et al.*, 2011]. In principle, steady state grain size evolves through a competition between dislocation-driven dynamic recrystallization

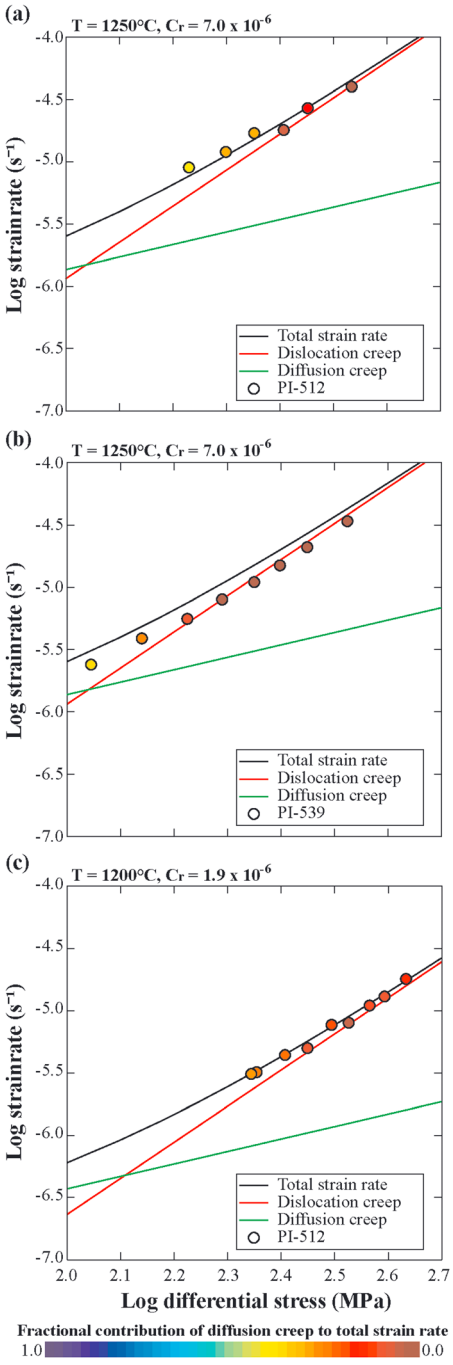

Figure 2. Log differential stress versus log strain rate plots for *Lawlis* [1998] 100 vol.% enstatite 450 MPa confining pressure deformation experiments (a) PI-512 at 1250°C, (b) PI-539 at 1250°C, and (c) PI-512 at 1200°C. Red lines show the dislocation creep flow law for orthoenstatite from *Lawlis* [1998]. Green lines show the diffusion creep flow law based on the rheological constraints (equation (5)). Black lines show the total strain rate, which is assumed to be the sum of the strain rates contributed by dislocation creep and diffusion creep. The mechanical data are plotted as solid circles in a color that represents the fractional contribution of diffusion creep to the total strain rate. The maximum contribution of diffusion creep to the total strain rate is 40%.

when the material deforms by dislocation creep, and grain growth when the material is deforming by other mechanisms such as diffusion creep [e.g., *Hall and Parmentier*, 2003]. *De Bresser et al.* [1998, 2001] argued that the piezometer and the field boundary between dislocation creep and diffusion creep should be similar because in an actively deforming rock the competing processes of dynamic recrystallization and grain-growth force the steady state grain size to converge towards the field boundary—the so-called field boundary hypothesis. Strictly, the physics of the field boundary and the grain-size piezometer are different; however, the interactions between underlying microphysical processes yield boundaries that fall in similar domains of parameter space. For many geologic materials it is found that the grain-size piezometers, plotted in stress-grain-size space, are sub-parallel to the field boundary and exhibit similar, weak temperature dependence [*Shimizu*, 1998; *Austin and Evans*, 2007].

Empirically calibrated grain-size piezometers are normally parameterized by a temperature-independent power law relationship [e.g., *Twiss*, 1977; *Karato et al.*, 1980; *Van der Wal et al.*, 1993; *Stipp and Tullis*, 2003; *Linckens et al.*, 2014]

$$\sigma = \alpha d^{-\beta} \tag{6}$$

where σ is stress in MPa and d is grain size in μm, and α and β are material-dependent constants. Parameters for the orthopyroxene grain-size piezometer of *Linckens et al.* [2014], which is derived from experiments and natural samples deformed between 1177°C and 1325°C, are given in Table 1.

On the field boundary between two deformation mechanisms the strain rate for each deformation mechanism is equal (equation (2)). Hence,

$$A_{dis}\sigma^{n_{dis}} \exp\left(-\frac{H_{dis}}{RT}\right) = A_{gss}\sigma^{n_{gss}} d^{-p} \exp\left(-\frac{H_{gss}}{RT}\right) \tag{7}$$

Again, we simplify the GSS flow law by combining pre-exponential A_{gss} and the temperature-dependent Arrhenius term (exp $(-H_{gss}/RT)$) into a single temperature-dependent variable $C_m(T)$, where the subscript "m" refers to the microstructural approach. As with the rheological approach, we assume that the GSS deformation mechanism is diffusion creep, and that n_{gss} is 1 [e.g., *Coble*, 1963]. In this calculation we do not assume a grain-size exponent a priori:

$$A_{dis}\sigma^{n_{dis}} \exp\left(-\frac{H_{dis}}{RT}\right) = C_m(T)\sigma d^{-p} \tag{8}$$

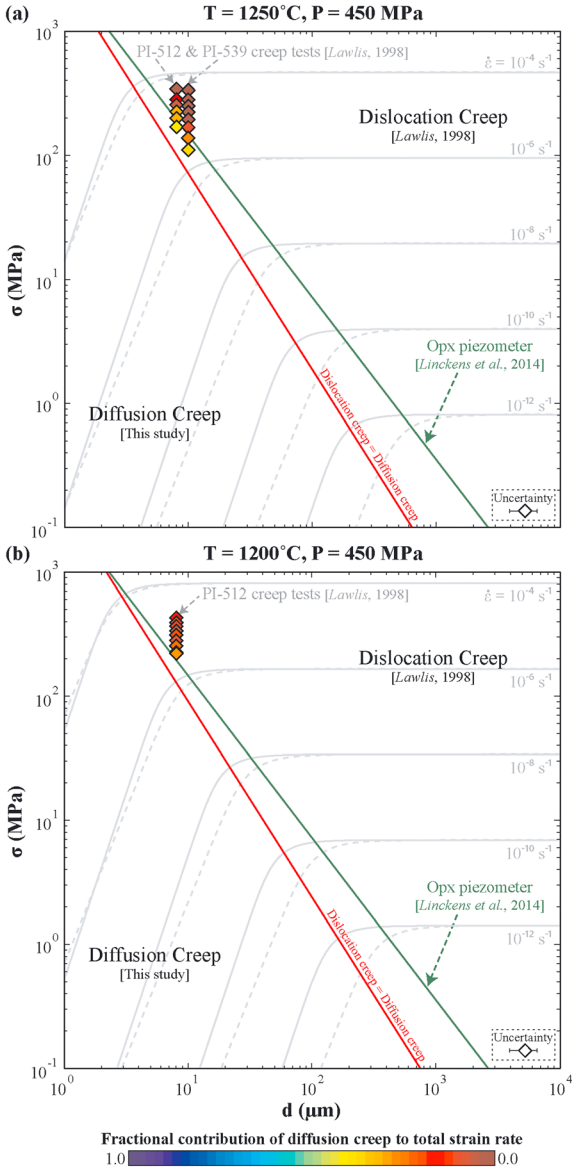

Figure 3. Deformation mechanism maps for orthopyroxene at 450 MPa confining pressure and (a) 1250°C and (b) 1200°C. Contours of constant strain rate were calculated using flow law parameters provided in Table 1. Flow laws for dislocation creep are from *Lawlis* [1998]. Flow laws for diffusion creep were calculated using independent microstructural (dashed) and rheological (solid) approaches. The orthopyroxene (Opx) piezometer of *Linckens et al.* [2014] represents the diffusion creep/dislocation creep field boundary inferred from microstructures. The light red lines denote the field boundary inferred from the mechanical data of *Lawlis* [1998]. Data from the *Lawlis* [1998] experiments are plotted as solid diamonds in a color that represents the fractional contribution of diffusion creep to the strain rate of the creep tests. For clarity purposes, the data for PI-539 at T = 1250°C in Figure 3a is offset to slightly higher grain size.

Solving for σ yields an expression that represents the field boundary of a deformation mechanism map in stress-grain-size space:

$$\sigma = \left[\frac{C_m(T)}{A_{dis}\exp\left(-\frac{H_{dis}}{RT}\right)}\right]^{1/(n_{dis}-1)} d^{-p/(n_{dis}-1)} \quad (9)$$

At constant temperature, the grain-size piezometer (equation (6)) and the field boundary (equation (9)) are both lines on a plot of log(σ) versus log(d). Following the field boundary hypothesis, we equate the relation for the grain-size piezometer to the functional form of the deformation mechanism field boundary, by combining equations (6) and (9), and solving for p and $C_m(T)$:

$$p = \beta(n_{dis} - 1) \quad (10)$$

$$C_m(T) = A_{dis}\exp\left(-\frac{H_{dis}}{RT}\right)\alpha^{(n_{dis}-1)} \quad (11)$$

p is calculated to be 2.49, which falls between the predicted grain-size sensitivity for Nabarro-Herring creep and Coble creep [e.g., *Poirier*, 1985]. Using these calculated values for p and $C_m(T)$, the resulting grain-size sensitive flow law (right-hand side of equations (7) and (8)) is used to calculate an additional set of field boundaries and strain rate contours for the deformation mechanism maps (Figure 3).

3. Results

Figure 3 shows deformation mechanism maps calculated for temperatures of 1200°C and 1250°C using both the microstructural and rheological constraints for diffusion creep and the *Lawlis* [1998] flow law parameters for dislocation creep. The mechanical data from the *Lawlis* [1998] experiments are plotted using the steady state stresses for each creep test and an average grain size inferred from backscatter electron micrographs of other experiments within the same study. Markers for each creep test are colored according to the fractional contribution of diffusion creep to $\dot{\varepsilon}_{tot}$ (Figure 3). For clarity, the markers for PI-539 are offset to a slightly larger grain size. In general, experiments at lower stresses have an increased contribution from diffusion creep. The maximum contribution to the total strain rate from diffusion creep is 40%. Field boundaries determined using the two methods are sub-parallel and separated in grain size by a factor of only 2–5. The microstructural constraint predicts that the field boundary occurs at larger stresses or grain sizes than the rheological constraint.

4. Discussion

Detailed knowledge of mantle rheology is the key to understanding the existence and longevity of plate tectonics on planetary bodies [*Moresi and Solomatov*, 1998; *Bercovici*, 2003]. In numerical or theoretical studies of mantle deformation, olivine flow laws [e.g., *Karato and Wu*, 1993; *Hirth and Kohlstedt*, 2003] are generally used to simulate the rheology of the upper mantle [e.g., *Moresi and Solomatov*, 1998; *King and Ritsema*, 2000; *Précigout and Gueydan*, 2009; *Chu and Korenaga*, 2012; *Hidas et al*., 2013]. Although a few studies have successfully implemented two-phase rheology into models of plate tectonics [*Bercovici and Ricard*, 2013, 2014] the role of orthopyroxene is not often considered. Justification for this simplification is based on the following: (1) the fact that olivine is the most abundant mineral in an upper mantle of pyrolitic composition [*Ringwood*, 1975], (2) comparison of empirical high-temperature flow laws for orthopyroxene and olivine single crystals suggests that orthopyroxene is the stronger phase [*Durham and Goetze*, 1977; *Mackwell*, 1991], and (3) experimental and field-based studies on rocks of ultramafic compositions have shown that the viscosity of dunite and harzburgite is similar for orthopyroxene contents up to 15–30% [*Kohlstedt and Zimmerman*, 1996; *Tikoff et al*., 2010].

Many recent studies, particularly microstructural investigations of naturally deformed peridotite mylonites, have argued that orthopyroxene may play a more significant role in the deformation of the mantle, particularly in high-strain plate boundary regions [e.g., *Skemer and Karato*, 2008; *Skemer et al*., 2010; *Toy et al*., 2010]. Unlike more weakly deformed peridotite massifs [e.g., *Hoogerduijn Strating et al*., 1993; *Précigout et al*., 2013], the grain size in highly sheared mylonites is reduced, the olivine and pyroxene phases are often well mixed, and one or both phases are interpreted to deform by a grain-size sensitive mechanism such as diffusion creep or dislocation accommodated grain-boundary sliding [*Warren and Hirth*, 2006]. The mutual phase mixing of pyroxene and olivine is a critical process, suppressing grain growth by Zener pinning and promoting long-lived grain-size sensitive deformation, even as deformation conditions change [*Smith*, 1948; *Olgaard and Evans*, 1986; *Evans et al*., 2001; *Précigout et al*., 2007; *Herwegh et al*., 2011; *Linckens et al*., 2011b; *Michibayashi et al*., 2013; *Linckens et al*., 2014].

Unlike olivine, which is well characterized by experimental rock physics [e.g., *Durham and Goetze*, 1977; *Chopra and Paterson*, 1984; *Karato et al*., 1986; *Mei and Kohlstedt*, 2000a, 2000b; *Hansen et al*., 2011, 2012], orthopyroxene has received comparatively little attention. Two early studies [*Raleigh et al*., 1971 and *Ross and Nielsen*, 1978] derived flow laws for orthopyroxene at high pressure. However, the data in these experiments were likely biased by friction in the solid-medium cell. *Mackwell* [1991] conducted a more precise series of tests on single crystal orthopyroxene at high temperature and room pressure; however, at these conditions protoenstatite, rather than orthoenstatite, is the stable phase. The most extensive study of orthopyroxene composition rocks was conducted by *Lawlis* [1998]. These experiments, which were performed at high temperature and high pressure in a gas-medium apparatus, demonstrate distinct differences in the rheology of orthopyroxene deformed at 300 MPa and 450 MPa confining pressure. The contrast in rheology is attributed to the phase transition between protoenstatite and orthoenstatite [*Lawlis*, 1998; *Bystricky et al*., 2011]. There have been a few additional experimental studies on the rheology of orthopyroxene; however, all were conducted in the protoenstatite stability field, or at conditions that strongly favor dislocation creep [*Carter et al*., 1972; *Hitchings et al*., 1989; *Ji et al*., 2001; *Ohuchi et al*., 2011; *Tasaka et al*., 2013].

The rheological constraints in this study are derived from a small number of creep tests at low stresses performed by *Lawlis* [1998] where deviation from non-linear dislocation creep is observed (Figure 2). Although limited to a small parameter space, these data provide a valuable constraint to the conditions of onset of diffusion creep (Figure 3). To define a GSS flow law we are forced to select a particular model for deformation. For simplicity, we chose to assume that the deviation from the dislocation creep flow law was caused by the contribution of grain-boundary diffusion (Coble) creep, in which strain rate is proportional to stress and inversely proportional to grain size to the power of three [*Poirier*, 1985]. As the *Lawlis* [1998] experiments were conducted on samples with a narrow range of grain sizes, we cannot exclude the importance of other deformation mechanisms with different sensitivities to grain size and/or stress, such as Nabarro-Herring creep or dislocation-accommodated grain-boundary sliding. Our assumption that deformation took place by Coble creep places the field boundary at the smallest range of grain sizes and therefore represents the most conservative boundary to the conditions that favor GSS creep. The temperature sensitivity of the diffusion creep flow law is poorly constrained, with data separated by only 50°C. The

temperature dependence of C_r (equation (5) and Table 1) yields an activation enthalpy (H_{gss}) and pre-exponential constant (A_{gss}) of 486 kJ/mol and 3.4×10^{11} μm^3/MPa s, respectively. These values are reasonable and may be consistent with the activation enthalpy for grain boundary diffusivity of MgO in dry orthoenstatite (417 +/− 38 kJ/mol) determined by *Gardés and Heinrich* [2011]. However, further experimental study is needed to corroborate this value.

The microstructural approach used in this study builds on the field boundary hypothesis [*De Bresser et al*., 1998, 2001], which argues convincingly that dynamically recrystallized grain size should evolve toward the field boundary between dislocation creep and diffusion creep. Our application of the field boundary hypothesis is not rigorously correct, as we equate two physical relations, the field boundary and the recrystallized grain-size piezometer, which are grounded in different underlying physics. The physical basis of the grain-size piezometer is considered to arise from the dynamic balance between dislocation-driven dynamic recrystallization and some form of coarsening or grain boundary migration [e.g., *Derby and Ashby*, 1987; *Shimizu*, 1998]. On the other hand, the field boundary represents the conditions at which two deformation mechanisms contribute equally to the total strain rate and thus depends only on the microphysics of dislocation creep and diffusion creep [*Frost and Ashby*, 1982]. Although for many geologic materials the piezometer and the field boundary are similar [e.g., *Austin and Evans*, 2007; *Shimizu*, 2008] there is generally a small but significant deviation between the two, which may be related to the relative kinetics of dynamic recrystallization and grain growth [*Skemer and Karato*, 2007, 2008]. Although more rheological data are needed to validate this microstructural approach as applied to orthopyroxene, we assert that the orthopyroxene grain-size piezometer may provide a valuable first-order constraint on the location of the field boundary between dislocation and diffusion creep.

The rheological and microstructural approaches described here are complementary. While both share some common simplifications, such as the assumption that GSS deformation in orthopyroxene is a form of diffusion creep, the methodologies are independent. Therefore, it is significant that both methods yield similar results. For example, at 1250°C and a flow stress of 7 MPa, the critical grain size for the onset of diffusion creep is 45 μm and 100 μm using the rheological and microstructural constraints, respectively. Over a wide range of conditions, the difference between the two field boundaries is only a factor of 2–5, which is quite small in comparison to the range of grain sizes observed in Earth.

Through the application of olivine grain-size piezometers and seismological constraints, stress in the lithosphere has been estimated to be about 7–75 MPa [e.g., *Frohlich*, 2006; *Falus et al*., 2008; *Prieto et al*., 2013; *Behr and Hirth*, 2014]. Using the rheologically constrained diffusion creep flow law derived here, along with the dislocation creep flow law of *Lawlis* [1998] and the olivine flow laws of *Hirth and Kohlstedt* [2003] and *Hansen et al*. [2011], we can begin to assess the relative strengths of olivine and orthopyroxene at lithospheric conditions. At 1250°C, a flow stress of 7 MPa, and grain-sizes prescribed by the appropriate piezometers, orthopyroxene strain rates are nearly an order of magnitude greater than olivine strain rates. This contrast reflects both the intrinsic rheology of the two minerals, as well as the significant difference between their respective recrystallized grain size at constant stress conditions. Under conditions where the grain size of orthopyroxene and olivine is similar, for example in well-mixed ultramylonites, the contrast in rheology is reduced.

The deformation mechanism maps constructed in our study demonstrate that over a wide range of conditions orthopyroxene in the upper mantle may deform predominantly by a grain-size sensitive mechanism. Orthopyroxene with highly reduced grain size may be generated in peridotite by several chemical or deformation-induced processes, including (i) metamorphic reactions [e.g., *Newman et al*., 1999; *Toy et al*., 2010], (ii) fluxing of a reactive melt [*Dijkstra et al*., 2002], (iii) dynamic recrystallization when grain growth can be suppressed through the presence of secondary phases [*Smith*, 1948; *Olgaard and Evans*, 1986; *Evans et al*., 2001; *Précigout et al*., 2007; *Herwegh et al*., 2011; *Linckens et al*., 2011b; *Michibayashi et al*., 2013], or (iv) cataclasis [*Vissers et al*., 1997]. Abundant geological evidence suggests that grain-size sensitive deformation of orthopyroxene plays a significant role in the deformation of the upper mantle, particularly in highly deformed ductile shear zones where mutual grain-size pinning influences both olivine and orthopyroxene rheology [*Boullier and Gueguen*, 1975; *Dijkstra et al*., 2002; *Skemer and Karato*, 2008; *Skemer et al*., 2010; *Toy et al*., 2010; *Linckens et al*., 2011a; *Hidas et al*., 2013]. As the transition from dislocation creep to grain-size sensitive creep is expected to promote rheological weakening [*Rutter and Brodie*, 1988], orthopyroxene may likewise play a pivotal role in shear localization phenomena along plate boundaries.

5. Conclusions

Deformation mechanism maps for orthopyroxene, and the underlying flow laws, constructed using independent rheological and microstructural methods, show a wide range of conditions where GSS creep is an important deformation mechanism in Earth. The field boundaries in the deformation mechanism maps calculated by the two approaches are sub-parallel and separated in grain size by a factor of only 2–5. Based on our findings it is concluded that at upper mantle conditions the transition from dislocation creep to grain-size sensitive creep in orthopyroxene occurs at a grain-size range of ~150–500 μm, within the normal grain-size range for mylonites and ultramylonites. Orthopyroxene, as the second-most abundant mineral phase in the upper mantle, may play an essential role in the deformation of the crust and upper mantle, both as a pinning phase in the deformation of composite materials, and due to its intrinsic weakness when deforming by GSS creep.

Acknowledgments

The Matlab® code used to construct the deformation mechanism maps of Figure 3 and calculate the curves of Figure 2, and the electron backscatter diffraction (EBSD) data used to construct Figure 1 are available for download at http://espm.wustl.edu/wp-content/uploads/Bruijn_Skemer_GRL_data.zip. This study was supported by NSF EAR-0911289 (to PS) and a grant from the McDonnell Center for Space Sciences, Washington University in St. Louis (to RHCB). We thank David Bercovici and Lars Hansen for their constructive and thoughtful reviews.

The Editor thanks David Bercovici and Lars Hansen for their assistance in evaluating this paper.

References

Austin, N. J., and B. Evans (2007), Paleowattmeters: A scaling relation for dynamically recrystallized grain size, *Geology*, *35*(4), 343–346, doi:10.1130/G23244A.1.

Behr, W. M., and G. Hirth (2014), Rheological properties of the mantle lid beneath the Mojave region in southern California, *Earth Planet. Sci. Lett.*, *393*, 60–72, doi:10.1016/j.epsl.2014.02.039.

Bercovici, D. (2003), The generation of plate tectonics from mantle convection, *Earth Planet. Sci. Lett.*, *205*(3–4), 107–121, doi:10.1016/S0012-821X(02)01009-9.

Bercovici, D., and Y. Ricard (2005), Tectonic plate generation and two-phase damage: Void growth versus grain size reduction, *J. Geophys. Res.*, *110*, B03401, doi:10.1029/2004JB003181.

Bercovici, D., and Y. Ricard (2013), Generation of plate tectonics with two-phase grain-damage and pinning: Source–sink model and toroidal flow, *Earth Planet. Sci. Lett.*, *365*, 275–288, doi:10.1016/j.epsl.2013.02.002.

Bercovici, D., and Y. Ricard (2014), Plate tectonics, damage and inheritance, *Nature*, *508*, 513–516, doi:10.1038/nature13072.

Boudier, F. (1978), Structure and petrology of the Lanzo peridotite massif (Piedmont Alps), *GSA Bull.*, *89*(10), 1574–1591, doi:10.1130/0016-7606(1978)89<1574:SAPOTL>2.0.CO;2.

Boullier, A. M., and Y. Gueguen (1975), SP-Mylonites: Origin of some mylonites by superplastic flow, *Contrib. Mineral. Petrol.*, *50*(2), 93–104, doi:10.1007/BF00373329.

Bystricky, M., J. D. Lawlis, S. J. Mackwell, F. Heidelbach, and P. C. Ratteron (2011), High-Temperature Deformation of Enstatite Aggregates, paper presented at American Geophysical Union fall meeting, AGU, San Francisco, Calif.

Carter, N. L., D. W. Baker, and R. P. George (1972), Seismic anisotropy, flow, and constitution of the upper mantle, in *Flow and Fracture of Rocks*, *Geophys. Monogr. Ser.*, vol. 16, edited by H. C. Heard et al., pp. 167–190, AGU, Washington, D. C.

Chopra, P. N., and M. S. Paterson (1984), The role of water in the deformation of dunite, *J. Geophys. Res.*, *89*(B9), 7861–7876, doi:10.1029/JB089iB09p07861.

Christensen, N. I., and S. M. Lundquist (1982), Pyroxene orientation within the upper mantle, *GSA Bull.*, *93*(4), 279–288, doi:10.1130/0016-7606(1982)93<279:POWTUM>2.0.CO;2.

Chu, X., and J. Korenaga (2012), Olivine rheology, shear stress, and grain growth in the lithospheric mantle: Geological constraints from the Kaapvaal craton, *Earth Planet. Sci. Lett.*, *333*, 52–62, doi:10.1016/j.epsl.2012.04.019.

Coble, R. L. (1963), A model for boundary diffusion controlled creep in polycrystalline materials, *J. Appl. Phys.*, *34*(6), 1679–1682, doi:10.1063/1.1702656.

De Bresser, J. H. P., C. J. Peach, J. P. J. Reijs, and C. J. Spiers (1998), On dynamic recrystallization during solid state flow: Effects of stress and temperature, *Geophys. Res. Lett.*, *25*(18), 3457–3460, doi:10.1029/98GL02690.

De Bresser, J., J. Ter Heege, and C. J. Spiers (2001), Grain size reduction by dynamic recrystallization: Can it result in major rheological weakening?, *Int. J. Earth Sci.*, *90*(1), 28–45, doi:10.1007/s005310000149.

Derby, B., and M. F. Ashby (1987), On dynamic recrystallisation, *Scr. Metal.*, *21*(6), 879–884, doi:10.1016/0036-9748(87)90341-3.

Dijkstra, A. H., M. R. Drury, R. L. M. Vissers, and J. Newman (2002), On the role of melt-rock reaction in mantle shear zone formation in the Othris Peridotite Massif (Greece), *J. Struct. Geol.*, *24*(9), 1431–1450, doi:10.1016/S0191-8141(01)00142-0.

Durham, W. B., and C. Goetze (1977), Plastic flow of oriented single crystals of olivine: 1. Mechanical data, *J. Geophys. Res.*, *82*(36), 5737–5753, doi:10.1029/JB082i036p05737.

Etheridge, M. A. (1975), Deformation and recrystallisation of orthopyroxene from the Giles Complex, Central Australia, *Tectonophysics*, *25*(1–2), 87–114, doi:10.1016/0040-1951(75)90012-8.

Evans, B., J. Renner, and G. Hirth (2001), A few remarks on the kinetics of static grain growth in rocks, *Int. J. Earth Sci.*, *90*(1), 88–103, doi:10.1007/s005310000150.

Falus, G., A. Tommasi, J. Ingrin, and C. Szabó (2008), Deformation and seismic anisotropy of the lithospheric mantle in the southeastern Carpathians inferred from the study of mantle xenoliths, *Earth Planet. Sci. Lett.*, *272*(1–2), 50–64, doi:10.1016/j.epsl.2008.04.035.

Frohlich, C. (2006), *Deep Earthquakes*, Cambridge Univ. Press, Cambridge, U. K.

Frost, H. J., and M. F. Ashby (Eds) (1982), *Deformation-Mechanism Maps: The Plasticity and Creep of Metals and Ceramics*, Pergamon Press, Oxford, U. K.

Gardés, E., and W. Heinrich (2011), Growth of multilayered polycrystalline reaction rims in the MgO–SiO2 system, part II: Modelling, *Contrib. Mineral. Petrol.*, *162*(1), 37–49, doi:10.1007/s00410-010-0581-4.

Hall, C. E., and E. M. Parmentier (2003), Influence of grain size evolution on convective instability, *Geochem. Geophys. Geosyst.*, *4*(3), 1029, doi:10.1029/2002GC000308.

Hansen, L. N., M. E. Zimmerman, and D. L. Kohlstedt (2011), Grain boundary sliding in San Carlos olivine: Flow law parameters and crystallographic-preferred orientation, *J. Geophys. Res.*, *116*, B08201, doi:10.1029/2011JB008220.

Hansen, L. N., M. E. Zimmerman, and D. L. Kohlstedt (2012), Laboratory measurements of the viscous anisotropy of olivine aggregates, *Nature*, *492*(7429), 415–418, doi:10.1038/nature11671.

Herwegh, M., J. Linckens, A. Ebert, A. Berger, and S. H. Brodhag (2011), The role of second phases for controlling microstructural evolution in polymineralic rocks: A review, *J. Struct. Geol.*, *33*, 1728–1750, doi:10.1016/j.jsg.2011.08.011.

Hidas, K., C. J. Garrido, A. Tommasi, J. A. Padrón-Navarta, M. Thielmann, Z. Konc, E. Frets, and C. Marchesi (2013), Strain localization in pyroxenite by reaction-enhanced softening in the shallow subcontinental lithospheric mantle, *J. Petrol.*, *54*(10), 1997–2031, doi:10.1093/petrology/egt039.

Hirth, G., and D. L. Kohlstedt (2003), Rheology of the mantle wedge, in *Inside the Subduction Factory*, *Geophys. Monogr. Ser.*, vol. 138, edited by J. Eiler, AGU, Washington, D. C.

Hitchings, R. S., M. S. Paterson, and J. Bitmead (1989), Effects of iron and magnetite additions in olivine-pyroxene rheology, *Phys. Earth Planet. Inter.*, *55*(3-4), 277–291, doi:10.1016/0031-9201(89)90076-9.

Hoogerduijn Strating, E. H., E. Rampone, G. B. Piccardo, M. R. Drury, and R. L. M. Vissers (1993), Subsolidus Emplacement of Mantle Peridotites during Incipient Oceanic Rifting and Opening of the Mesozoic Tethys (Voltri Massif, NW Italy), *J. Petrol.*, *34*(5), 901–927, doi:10.1093/petrology/34.5.901.

Ji, S., Z. Wang, and R. Wirth (2001), Bulk flow strength of forsterite–enstatite composites as a function of forsterite content, *Tectonophysics*, *341*(1–4), 69–93, doi:10.1016/S0040-1951(01)00191-3.

Kanagawa, K., H. Shimano, and Y. Hiroi (2008), Mylonitic deformation of gabbro in the lower crust: A case study from the Pankenushi gabbro in the Hidaka metamorphic belt of central Hokkaido, Japan, *J. Struct. Geol.*, *30*(9), 1150–1166, doi:10.1016/j.jsg.2008.05.007.

Karato, S., and P. Wu (1993), Rheology of the upper mantle: A synthesis, *Science*, *260*(5109), 771–778, doi:10.1126/science.260.5109.771.

Karato, S., M. Toriumi, and T. Fujii (1980), Dynamic recrystallization of olivine single crystals during high-temperature creep, *Geophys. Res. Lett.*, *7*(9), 649–652, doi:10.1029/GL007i009p00649.

Karato, S.-I., M. S. Paterson, and J. D. Fitz Gerald (1986), Rheology of synthetic olivine aggregates: Influence of grain size and water, *J. Geophys. Res.*, *91*(B8), 8151–8176, doi:10.1029/JB091iB08p08151.

King, S. D., and J. Ritsema (2000), African hot spot volcanism: Small-scale convection in the upper mantle beneath cratons, *Science*, *290*(5494), 1137–1140, doi:10.1126/science.290.5494.1137.

Kohlstedt, D. L., and J. B. Vander Sande (1973), Transmission electron microscopy investigation of the defect microstructure of four natural orthopyroxenes, *Contrib. Mineral. Petrol.*, *42*(2), 169–180, doi:10.1007/BF00371506.

Kohlstedt, D. L., and M. E. Zimmerman (1996), Rheology of partially molten mantle rocks, *Annu. Rev. Earth Planet. Sci.*, *24*, 41–62, doi:10.1146/annurev.earth.24.1.41.

Lawlis, J. D. (1998), High temperature creep of synthetic olivine-enstatite aggregates, PhD thesis, Dep. of Geosciences, Penn. State Univ., State College, Pa.

Linckens, J., M. Herwegh, O. Müntener, and I. Mercolli (2011a), Evolution of a polymineralic mantle shear zone and the role of second phases in the localization of deformation, *J. Geophys. Res.*, *116*, B06210, doi:10.1029/2010JB008119.

Linckens, J., M. Herwegh, and O. Müntener (2011b), Linking temperature estimates and microstructures in deformed polymineralic mantle rocks, *Geochem. Geophys. Geosyst.*, *12*, Q08004, doi:10.1029/2011GC003536.

Linckens, J., R. H. C. Bruijn, and P. Skemer (2014), Dynamic recrystallization and phase mixing in experimentally deformed peridotite, *Earth Planet. Sci. Lett.*, *388*, 134–142, doi:10.1016/j.epsl.2013.11.037.

Mackwell, S. J. (1991), High-temperature rheology of enstatite: Implications for creep in the mantle, *Geophys. Res. Lett.*, *18*(11), 2027–2030, doi:10.1029/91GL02492.

Mei, S., and D. L. Kohlstedt (2000a), Influence of water on plastic deformation of olivine aggregates: 1. Diffusion creep regime, *J. Geophys. Res.*, *105*(B9), 21,457–21,469, doi:10.1029/2000JB900179.

Mei, S., and D. L. Kohlstedt (2000b), Influence of water on plastic deformation of olivine aggregates: 2. Dislocation creep regime, *J. Geophys. Res.*, *105*(B9), 21,471–21,481, doi:10.1029/2000JB900180.

Michibayashi, K., M. Suzuki, and N. Komori (2013), Progressive deformation partitioning and recrystallization of olivine in the lithospheric mantle, *Tectonophysics*, *587*, 79–88, doi:10.1016/j.tecto.2012.07.008.

Mocquet, A., P. Rosenblatt, V. Dehant, and O. Verhoeven (2011), The deep interior of Venus, Mars, and the Earth: A brief review and the need for planetary surface-based measurements, *Planet. Space Sci.*, *59*(10), 1048–1061, doi:10.1016/j.pss.2010.02.002.

Moresi, L., and V. Solomatov (1998), Mantle convection with a brittle lithosphere: Thoughts on the global tectonic styles of the Earth and Venus, *Geophys. J. Int.*, *133*(3), 669–682, doi:10.1046/j.1365-246X.1998.00521.x.

Newman, J., W. M. Lamb, M. R. Drury, and R. L. M. Vissers (1999), Deformation processes in a peridotite shear zone: Reaction-softening by an H2O-deficient, continuous net transfer reaction, *Tectonophysics*, *303*(1–4), 193–222, doi:10.1016/S0040-1951(98)00259-5.

Nicolas, A., J. L. Bouchez, F. Boudier, and J. C. Mercier (1971), Textures, structures and fabrics due to solid state flow in some European lherzolites, *Tectonophysics*, *12*(1), 55–86, doi:10.1016/0040-1951(71)90066-7.

Ohuchi, T., S. Karato, and K. Fujino (2011), Strength of single-crystal orthopyroxene under lithospheric conditions, *Contrib. Mineral. Petrol.*, *161*(6), 961–975, doi:10.1007/s00410-010-0574-3.

Olgaard, D. L., and B. Evans (1986), Effect of second-phase particles on grain growth in calcite, *J. Am. Ceram. Soc.*, *69*(11), C272–C277.

Poirier, J.-P. (1985), *Creep of Crystals: High-Temperature Deformation Processes in Metals, Ceramics, and Minerals*, Cambridge Earth Sci. Ser., Cambridge Univ. Press, Cambridge, U. K.

Précigout, J., and F. Gueydan (2009), Mantle weakening and strain localization: Implications for the long-term strength of the continental lithosphere, *Geology*, *37*(2), 147–150, doi:10.1130/G25239A.1.

Précigout, J., F. Gueydan, D. Gapais, C. J. Garrido, and A. Essaifi (2007), Strain localisation in the subcontinental mantle — A ductile alternative to the brittle mantle, *Tectonophysics*, *445*(3-4), 318–336, doi:10.1016/j.tecto.2007.09.002.

Précigout, J., F. Gueydan, C. J. Garrido, N. Cogné, and G. Booth-Rea (2013), Deformation and exhumation of the Ronda peridotite (Spain), *Tectonics*, *32*, 1011–1025, doi:10.1002/tect.20062.

Presnall, D. C. (1995), Phase diagrams of Earth-forming minerals, in *A Handbook of Physical Constants, Mineral Physics and Crystallography*, vol. 2, edited by T. J. Ahrens, pp. 248–268, AGU, Washington, D. C.

Prieto, G. A., M. Florez, S. A. Barrett, G. C. Beroza, P. Pedraza, J. F. Blanco, and E. Poveda (2013), Seismic evidence for thermal runaway during intermediate-depth earthquake rupture, *Geophys. Res. Lett.*, *40*, 6064–6068, doi:10.1002/2013GL058109.

Raimbourg, H., T. Toyoshima, Y. Harima, and G. Kimura (2008), Grain-size reduction mechanisms and rheological consequences in high-temperature gabbro mylonites of Hidaka, Japan, *Earth Planet. Sci. Lett.*, *267*(3-4), 637–653, doi:10.1016/j.epsl.2007.12.012.

Raleigh, C. B., S. H. Kirby, N. L. Carter, and H. G. Avé Lallemant (1971), Slip and the clinoenstatite transformation as competing rate processes in enstatite, *J. Geophys. Res.*, *76*(17), 4011–4022, doi:10.1029/JB076i017p04011.

Ringwood, A. E. (1975), *Composition and Petrology of the Earth's Mantle*, McGraw-Hill Int. Ser. Earth Planet. Sc., McGraw-Hill, New York, N. Y.

Ross, J. V., and K. C. Nielsen (1978), High-temperature flow of wet polycrystalline enstatite, *Tectonophysics*, *44*(1–4), 233–261, doi:10.1016/0040-1951(78)90072-0.

Rozel, A., Y. Ricard, and D. Bercovici (2011), A thermodynamically self-consistent damage equation for grain size evolution during dynamic recrystallization, *Geophys. J. Int.*, *184*(2), 719–728, doi:10.1111/j.1365-246X.2010.04875.x.

Rutter, E. H., and K. H. Brodie (1988), The role of tectonic grain size reduction in the rheological stratification of the lithosphere, *Geol. Rundsch.*, *77*(1), 295–307, doi:10.1007/BF01848691.

Sanloup, C., A. Jambon, and P. Gillet (1999), A simple chondritic model of Mars, *Phys. Earth Planet. Inter.*, *112*(1–2), 43–54, doi:10.1016/S0031-9201(98)00175-7.

Shimizu, I. (1998), Stress and temperature dependence of recrystallized grain size: A subgrain misorientation model, *Geophys. Res. Lett.*, *25*(22), 4237–4240, doi:10.1029/1998GL900136.

Shimizu, I. (2008), Theories and applicability of grain size piezometers: The role of dynamic recrystallization mechanisms, *J. Struct. Geol.*, *30*(7), 899–917, doi:10.1016/j.jsg.2008.03.004.

Skemer, P., and S. Karato (2007), Effects of solute segregation on the grain-growth kinetics of orthopyroxene with implications for the deformation of the upper mantle, *Phys. Earth Planet. Inter.*, *164*(3-4), 186–196, doi:10.1016/j.pepi.2007.06.011.

Skemer, P., and S. Karato (2008), Sheared lherzolite xenoliths revisited, *J. Geophys. Res.*, *113*, B07205, doi:10.1029/2007JB005286.

Skemer, P., I. Katayama, Z. Jiang, and S. Karato (2005), The misorientation index: Development of a new method for calculating the strength of lattice-preferred orientation, *Tectonophysics*, *411*(1–4), 157–167, doi:10.1016/j.tecto.2005.08.023.

Skemer, P., I. Katayama, and S. Karato (2006), Deformation fabrics of the Cima di Gagnone peridotite massif, Central Alps, Switzerland: Evidence of deformation at low temperatures in the presence of water, *Contrib. Mineral. Petrol.*, *152*(1), 43–51, doi:10.1007/s00410-006-0093-4.

Skemer, P. A., J. M. Warren, P. B. Kelemen, and G. Hirth (2010), Microstructural and rheological evolution of a mantle shear zone, *J. Petrol.*, *51*(1–2), 43–53, doi:10.1093/petrology/egp057.

Smith, C. S. (1948), Grains, phases, and interfaces: An interpration of microstructure, *Trans. AIME*, *175*, 15–51.

Soustelle, V., A. Tommasi, J. L. Bodinier, C. J. Garrido, and A. Vauchez (2009), Deformation and reactive melt transport in the mantle lithosphere above a large-scale partial melting domain: The Ronda Peridotite Massif, Southern Spain, *J. Petrol.*, *50*(7), 1235–1266, doi:10.1093/petrology/egp032.

Stipp, M., and J. Tullis (2003), The recrystallized grain size piezometer for quartz, *Geophys. Res. Lett.*, *30*(21), 2088, doi:10.1029/2003GL018444.

Tasaka, M., T. Hiraga, and M. E. Zimmerman (2013), Influence of mineral fraction on the rheological properties of forsterite + enstatite during grain-size-sensitive creep: 2. Deformation experiments, *J. Geophys. Res. Solid Earth*, *118*, 3991–4012, doi:10.1002/jgrb.50284.

Tikoff, B., C. E. Larson, J. Newman, and T. Little (2010), Field-based constraints on finite strain and rheology of the lithospheric mantle, Twin Sisters, Washington, *Lithosphere*, *2*(6), 418–422, doi:10.1130/L97.1.

Toy, V. G., J. Newman, W. Lamb, and B. Tikoff (2010), The role of pyroxenites in formation of shear instabilities in the mantle: Evidence from an ultramafic ultramylonite, Twin Sisters Massif, Washington, *J. Petrol.*, *51*(1–2), 55–80, doi:10.1093/petrology/egp059.

Twiss, R. J. (1977), Theory and applicability of a recrystallized grain size paleopiezometer, *Pure Appl. Geophys.*, *115*(1–2), 227–244, doi:10.1007/BF01637105.

Van der Wal, D., P. Chopra, M. R. Drury, and J. Fitz Gerald (1993), Relationships between dynamically recrystallized grain size and deformation conditions in experimentally deformed olivine rocks, *Geophys. Res. Lett.*, *20*(14), 1479–1482, doi:10.1029/93GL01382.

Vissers, R. L. M., M. R. Drury, J. Newman, and T. F. Fliervoet (1997), Mylonitic deformation in upper mantle peridotites of the North Pyrenean Zone (France): Implications for strength and strain localization in the lithosphere, *Tectonophysics*, *279*(1–4), 303–325, doi:10.1016/S0040-1951(97)00128-5.

Warren, J. M., and G. Hirth (2006), Grain size sensitive deformation mechanisms in naturally deformed peridotites, *Earth Planet. Sci. Lett.*, *248*, 438–450, doi:10.1016/j.epsl.2006.06.006.